Electronic Supplementary Information for

A Revised Mechanism of Band Gap Evolution of TMDC Nanotubes and Its Application to Janus TMDC Nanotubes: Negative Electron and Hole Compressibility

XiaoHan Wang,[a] YingChao Liu,[a] JinLong Ren,[a] KunPeng Dou,[*,a] XingQiang Shi[*,b] and RuiQin Zhang[*,c,d]

[a]College of Information Science and Engineering, Ocean University of China, Qingdao 266100, China

[b]College of Physics Science and Technology, Hebei University, Baoding 071002, China

[c]Department of Physics, City University of Hong Kong, Hong Kong SAR, China

[d]Beijing Computational Science Research Center, Beijing 100193, China

E-mail: doukunpeng@ouc.edu.cn, shixq20hbu@hbu.edu.cn, aprqz@cityu.edu.hk

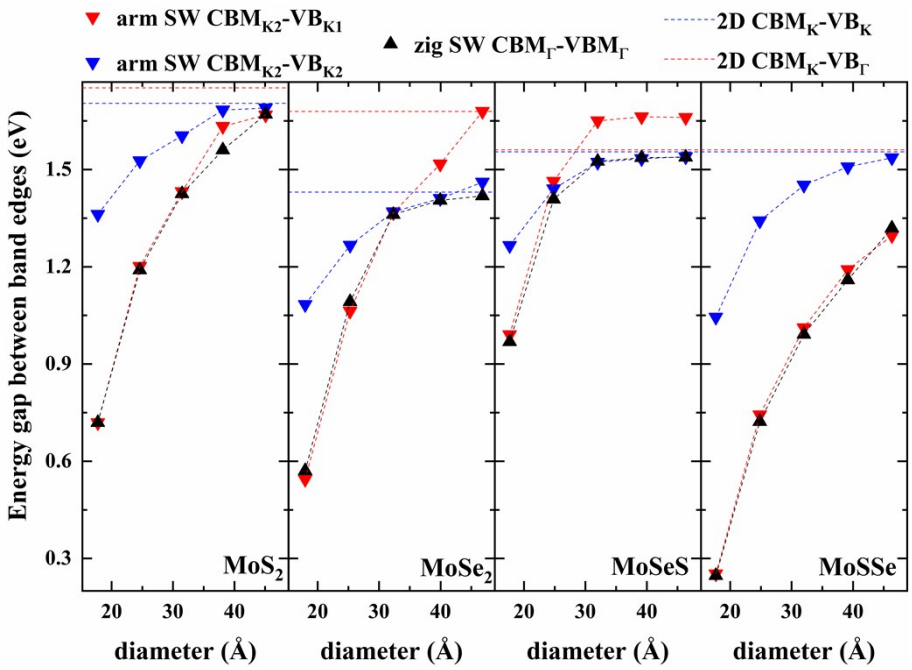

Fig. S1 Band gap evolution of TMDC nanotubes as a function of tube diameter for MoS_2, $MoSe_2$, Janus MoSeS and MoSSe tubes. The dashed horizontal lines denote the gap of the 2D monolayer counterpart.

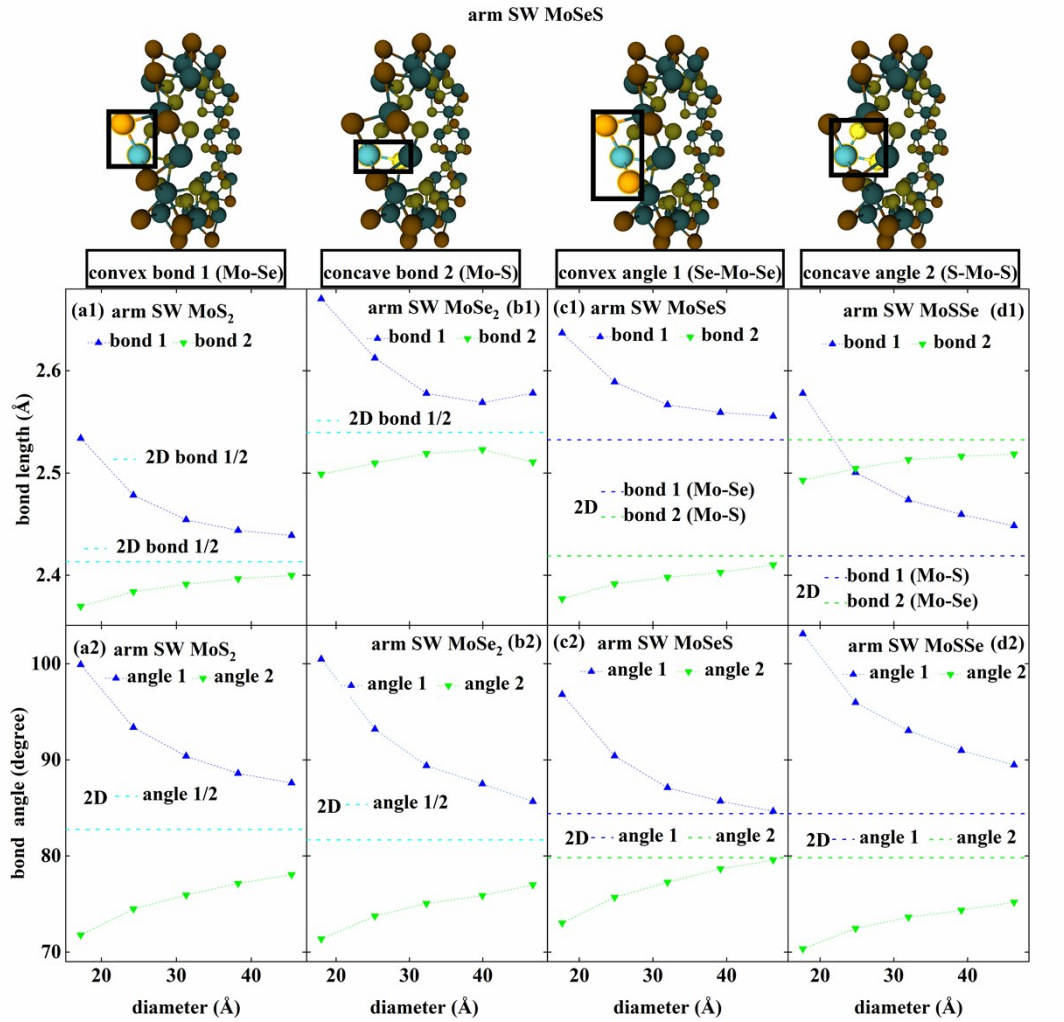

Fig. S2 Bond lengths and angles of armchair TMDC nanotubes as a function of tube diameter. The dashed horizontal lines denote the bond lengths and angles of corresponding monolayer counterpart. The definition numbers of bond and angle are schematized on the top panel with SW MoSeS NTs as the example. SW MoS_2 and MoSeS/MoSSe possess the same concave/convex chalcogen atom S and thus share the similar trend of geometrical variation on concave/convex side. The similar comparison can be made between SW $MoSe_2$ and Janus TMDC SW NT.

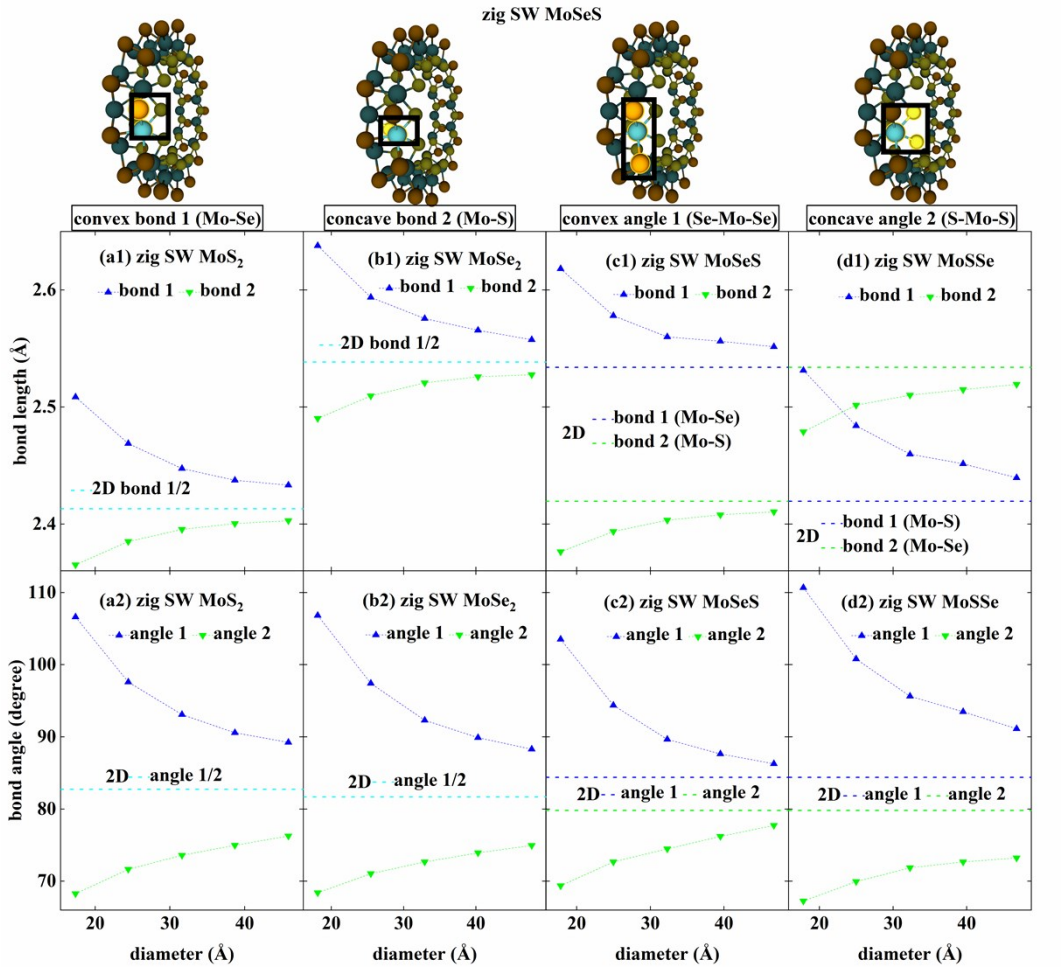

Fig. S3 Bond lengths and angles of zigzag TMDC nanotubes as a function of tube diameter. The dashed horizontal lines denote the bond lengths and angles of corresponding monolayer counterpart. The definition numbers of bond and angle are schematized on the top panel with SW MoSeS NTs as the example.

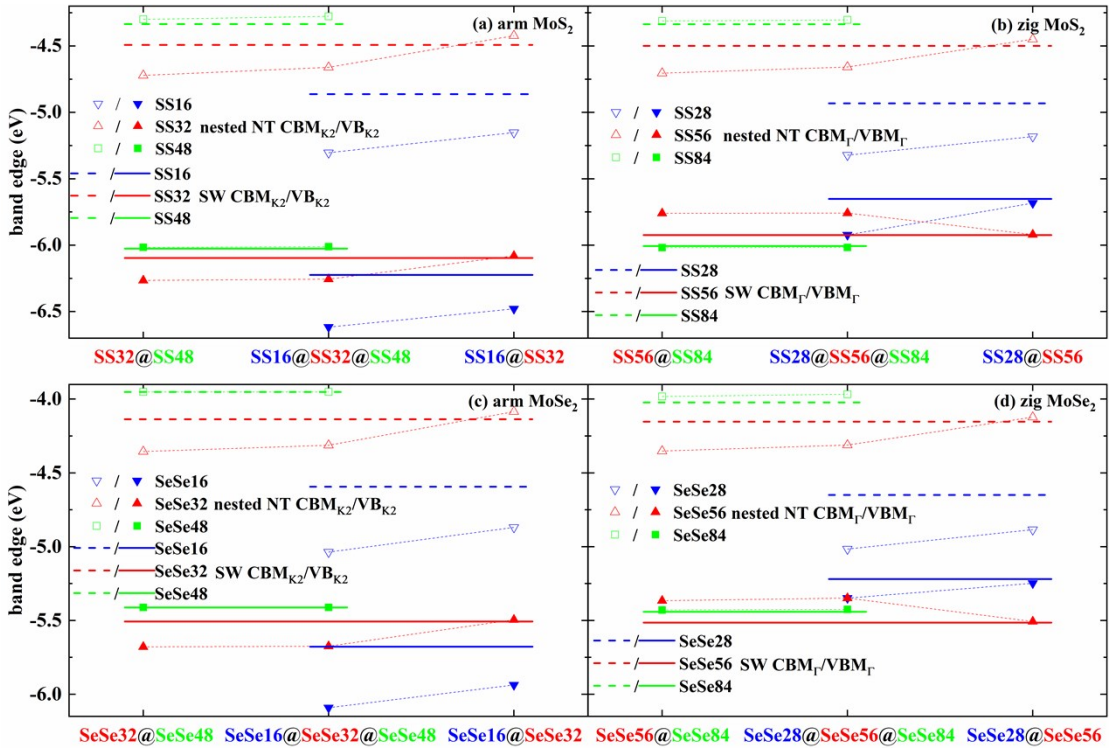

Fig. S4 Evolution of band edges for (a) armchair MoS_2 nanotubes, SS16, SS32 and SS48; (b) zigzag MoS_2 nanotubes, SS28, SS56 and SS84; (c) armchair $MoSe_2$ nanotubes, SeSe16, SeSe32 and SeSe48; (d) zigzag $MoSe_2$ nanotubes, SeSe28, SeSe56 and SeSe84 under nested circumstances. The horizontal solid and dashed lines indicate the band edges of isolated SW counterparts. The definition of short name for each NT can be found in Fig. 1 and the related text.

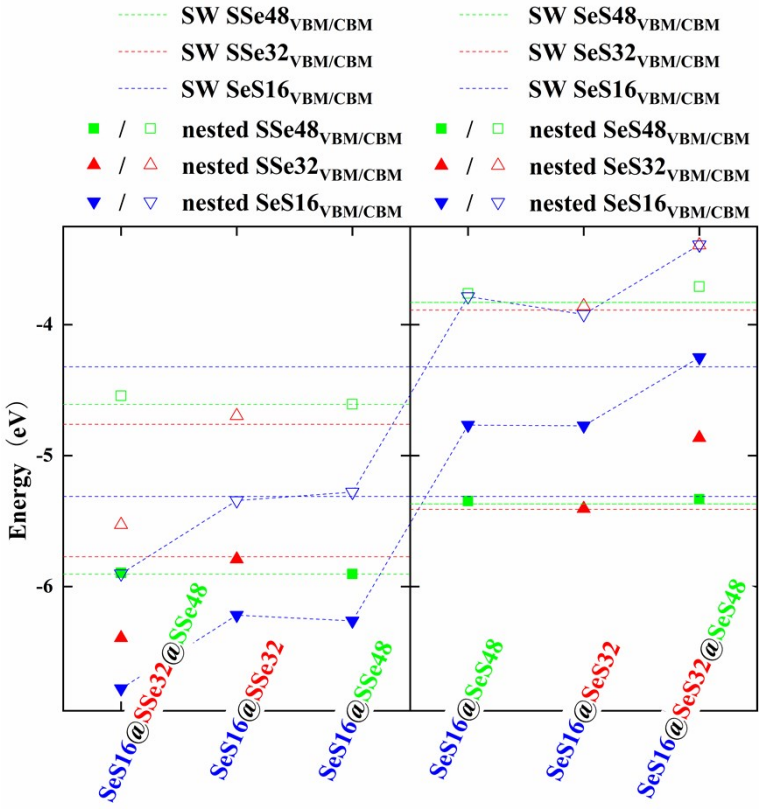

Fig. S5 Evolution of band edges for Janus armchair SeS16 nested in (a) armchair SSe NTs (b) armchair SeS NTs. The horizontal dashed lines indicate the band edges of isolated SW counterparts. The definition of short name for each NT can be found in Fig. 1 and the related text.

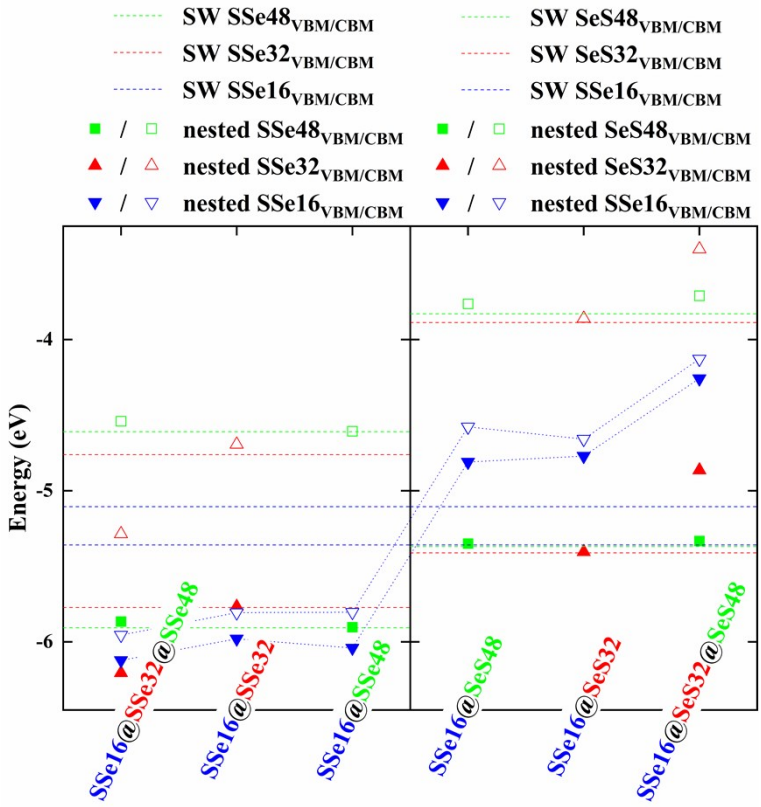

Fig. S6 Evolution of band edges for Janus armchair SSe16 nested in (a) armchair SSe NTs (b) armchair SeS NTs. The horizontal dashed lines indicate the band edges of isolated SW counterparts. The definition of short name for each NT can be found in Fig. 1 and the related text.

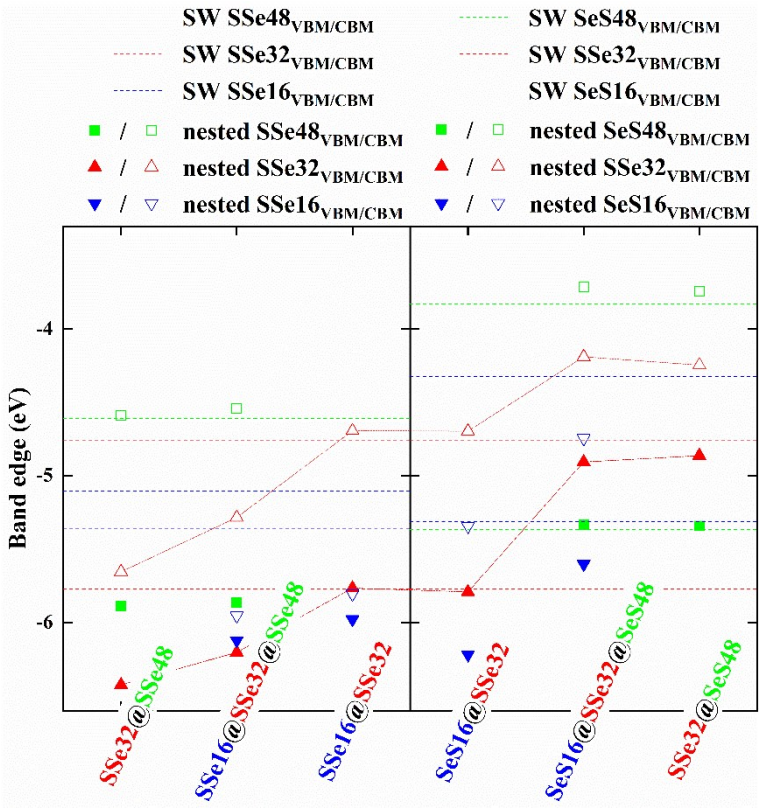

Fig. S7 Evolution of band edges for Janus armchair SSe32 nested in (a) armchair SSe NTs (b) armchair SeS NTs. The horizontal dashed lines indicate the band edges of isolated SW counterparts. The definition of short name for each NT can be found in Fig. 1 and the related text.

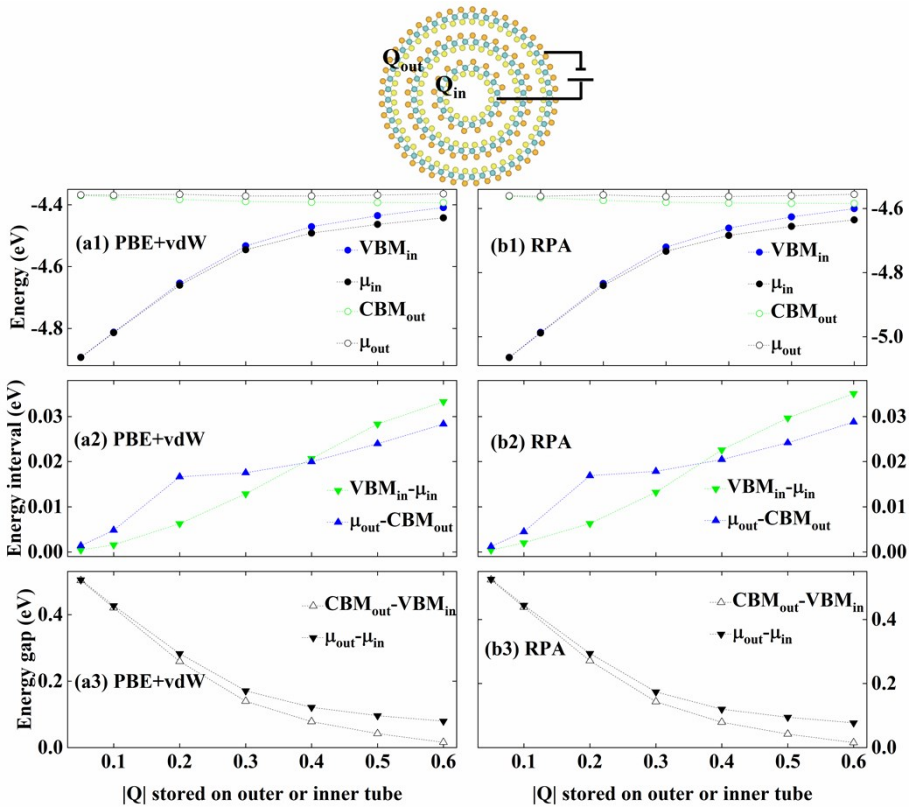

Fig. S8 Injected charge |Q| dependent (a1)-(b1) chemical potential and band edges; (a2)-(b2) energy integrating range for injected charge on each NT; (a3)-(b3) energy gap and chemical potential difference between inner NT and outer NT for Janus triple-wall (TW) SeS16@SeS32@SeS48 with PBE+vdw and RPA (Random Phase Approximation), respectively.

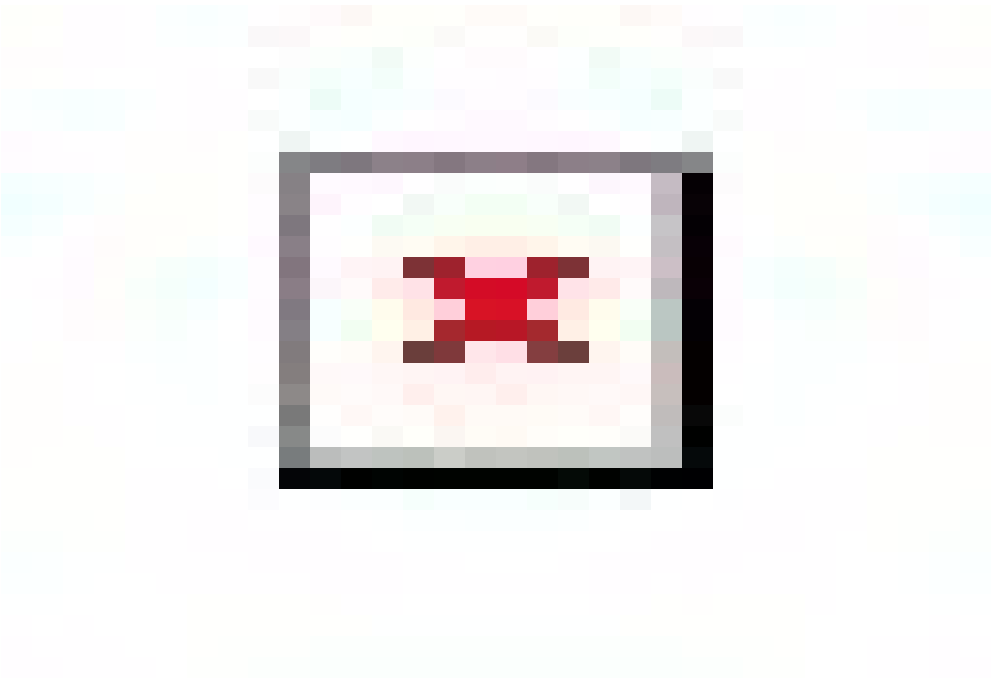

Fig. S9 Comparison of the evolution of (a) strain energy and (b) (c) band gap as a function of tube diameter.

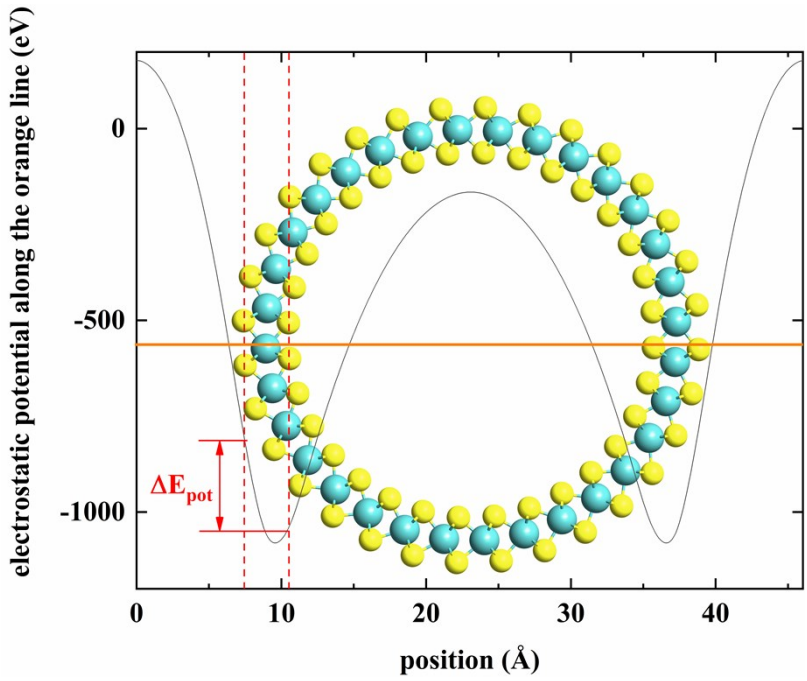

Fig. S10 Illustration of electrostatic potential difference (ΔE_{pot}) between convex and concave chalcogen atoms of armchair MoS_2 NT. The line-revolved electrostatic potential data can be collected by the post-processing script embedded in QuantumATK package. Both VASP and QuantumATK produce quantitatively the same values of

band gap as shown in Fig. S9 b and c.